Modelling of wind turbine gear stages for Digital Twin and real-time virtual sensing using bond graphs

Modelling of wind turbine gear stages for Digital Twin and real-time virtual sensing using bond graphs

F C Mehlan, E Pedersen, A R Nejad

Department of Marine Technology (IMT), Norwegian University of Science and Technology (NTNU), Trondheim, Norway

E-mail: felix.c.mehlan@ntnu.no

Abstract. In this paper a wind turbine high-speed gear stage model is developed for the purpose of real-time virtual sensing of gear and bearing loads in a Digital Twin framework. The model requirements are: accurate representation of gear meshing and shaft dynamics, high computational efficiency and compatibility with other Digital Twin components, such as physical sensors signals and virtual sensing methods. State equations are derived analytically using the Bond Graph method and implemented in the software 20sim for simulation. As opposed to standard multi-body simulation (MBS) software, 20sim allows for higher flexibility in implementing interfaces to other Digital Twin components. The model fidelity is close to state-of-the-art MBS models considering 6 DOF body motion, however a simplified gear contact formulation is used, which assumes ideal kinematic meshing. Nonetheless, the Bond Graph model is able to accurately reproduce the inhomogeneous load distribution over the tooth flank, as well as the cyclic compression and decompression for each meshing period. The results suggest that the presented model is capable of monitoring fatigue loads in gear contacts and bearings in a Digital Twin framework.

1. Introduction

Digital Twin (DT) is an emerging technology fueled by advances in information and communication technologies with many proposed applications in prognostics and health management (PHM). Especially the offshore wind industry could benefit from DT solutions to increase reliability and availability, and reduce unscheduled, expensive down times [1]. DT can be defined as a 'virtual representation of a physical asset enabled through data and simulators for real-time prediction, optimization, monitoring, controlling, and improved decision making' [2]. We envision a DT framework loosely based on the model of Tao et al. [3] to facilitate predictive maintenance (PdM) strategies in wind turbine drivetrains. The central components of the DT framework are the *Virtual model*, *Data* and *Decision support* (Fig. 1).

Data that can be leveraged in wind turbines include process, operational or organizational data, e.g. sensor measurements of the drivetrain condition monitoring system (CMS) and the Supervisory Control and Data Acquisition (SCADA) system. The *virtual model* is a virtual representation, that experiences the same environment as its physical counterpart and evolves over its life cycle. To ensure that the virtual and physical wind turbines are synchronized at all times, the virtual model is supplied with real-time, physical measurements and updated using system identification [4] and state estimation techniques [5]. *Decision support* is a collective term for services that the DT provides to assist in the operator's maintenance or control decisions.

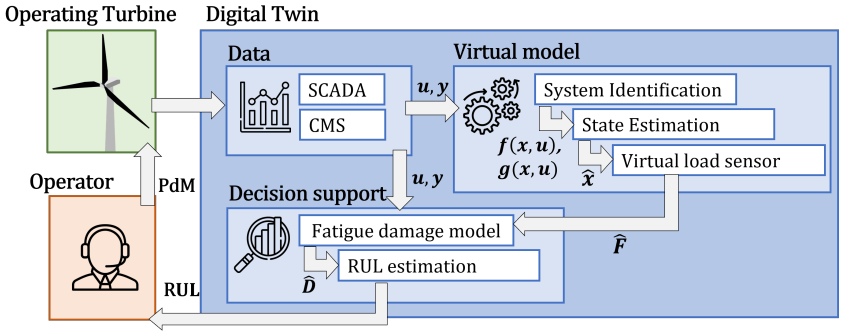

Figure 1. Digital Twin framework for predictive maintenance of wind turbine drivetrains.

Focus of our research is online monitoring of gear and bearing loads through virtual sensors and subsequent estimation of the remaining useful life (RUL) using fatigue damage models.
This study is concerned with developing a dynamic simulation model of a wind turbine high-speed gear stage to fit such a DT framework. The most essential model requirements are formulated based on Moyne et al. [6]:

- *Accuracy* in the representation of gear meshing and shaft dynamics
- *Computational efficiency* to enable real-time simulation
- *Interoperability* to interact with other DT-components, such as physical sensor signals and virtual sensing methods
- *Maintainability* to update model properties and match physical changes, such as material degradation

The task of balancing model accuracy and computational speed involves finding the optimal fidelity. Guidelines on modelling of wind turbine drivetrains are reported by Guo et al. [7], where recommendations on the degrees of freedom (DoF) for each moving drivetrain component, consideration of body flexibility and the fidelity of gear contact and bearing formulations are given, which concludes to a relatively high model fidelity. Hence, state-of-the-art multi-body simulation (MBS) models of wind turbine drivetrains including virtual test benches [8] and academic reference models [9, 10] are generally not capable of real-time simulation. Developing efficient Reduced Order Models (ROM) is identified as one of the major challenges in Predictive Maintenance and Condition Monitoring [11]. ROM are constructed either as data-driven surrogate models [12] or by physical simplification. In this study a simplified gear contact formulation is developed.
Secondly, to satisfy the requirements of interoperability with other DT-components, appropriate interfaces must be implemented. For instance, the virtual load sensor in the decision support component must be supplied with a mathematical description of the virtual model, which is elaborated further in Sec. 2.4. However, commercial MBS software including SIMPACK [13] and ADAMS only support the export of linearized models (state-space representation), which is insufficient to represent the highly non-linear dynamics of drivetrains [5].
Similar shortcomings of MBS software are identified concerning the model's maintainability. The DT paradigm requires the virtual model to evolve along its physical counterpart and be updated to match physical changes, such as material fatigue or component faults. While parametric updating is possible in MBS software, it is challenging to model gear and bearing faults due to restricted access to the respective component subroutines.
In this study a wind turbine gear stage model is developed with respect to the above mentioned

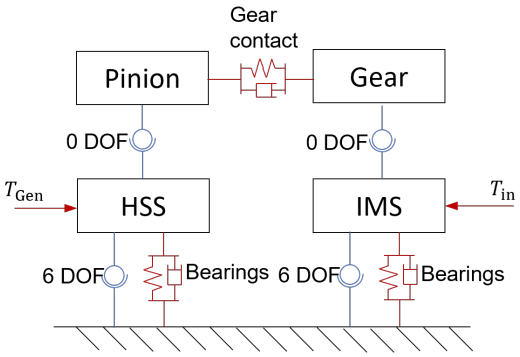

Figure 2. Gear stage model topology

DT requirements. The Bond Graph (BG) method, a graphical, energy-based modelling language [14], is employed to construct the model and derive state equations.

2. Methodology

2.1. Bond graph theory

BG is an energy-based, graphical modelling language that bridges the gap between purely equation-based modelling approaches and diagram techniques such as electrical circuit diagrams[14]. The universal currency of BG are the multi-physical effort $e(t)$ and flow $f(t)$ variables, which multiply to the instantaneous power $P(t)$. In the mechanical domain, for example, the energy variables are force and velocity, but the BG method also extends to other physical domains. The system is divided into components according to their capability of energy storage, dissipation or transmission. Kinetic and potential energy storage is represented by I- an C-elements, energy dissipation by R-elements and lossless energy transformation by TF-elements. The components are interconnected with power bonds representing the energy exchange. Power bonds are denoted with half arrows and define both the sign of the power by the arrow orientation and the causality of effort and flow variables with an orthogonal stroke. Causality determines whether variables are considered as input or output in the respective BG elements. The BG method is selected as modelling approach for the following reasons: First, it provides a systematic approach to deriving state equations for numerical simulation, while maintaining the physical structure of the system. Second, BG is not limited to any physical domain. Hence, other wind turbines components, for instance generator and converter, could be developed and integrated in the same framework. Third, the causality of state variables is visible in the BG structure, which eases the identification and prevention of algebraic loops that are detrimental to computational speed.

2.2. Reference model

The BG model in this study is based on a reference model of the NREL 5MW baseline wind turbine and respective gearbox [9] in terms of parameterization and topology. The reference model implemented in MBS software SIMPACK satisfies general guidelines on model fidelity [7] and is the basis for validation of the BG model's dynamics (Sec. 3). Parameter values of both models are listed in Tabs. 1 and 2, and the overall topology is shown in Fig. 2. The scope is limited to the high-speed stage, a helical gear stage with the bodies of intermediate speed shaft (IMS), high-speed shaft (HSS), gear wheel and pinion. Both gear shafts are considered rigid bodies with six degrees of freedom (DOF). Each shaft is supported by one cylindrical roller bearing (-A) and two tapered roller bearings (-B,-C), which are modelled as spring-damper

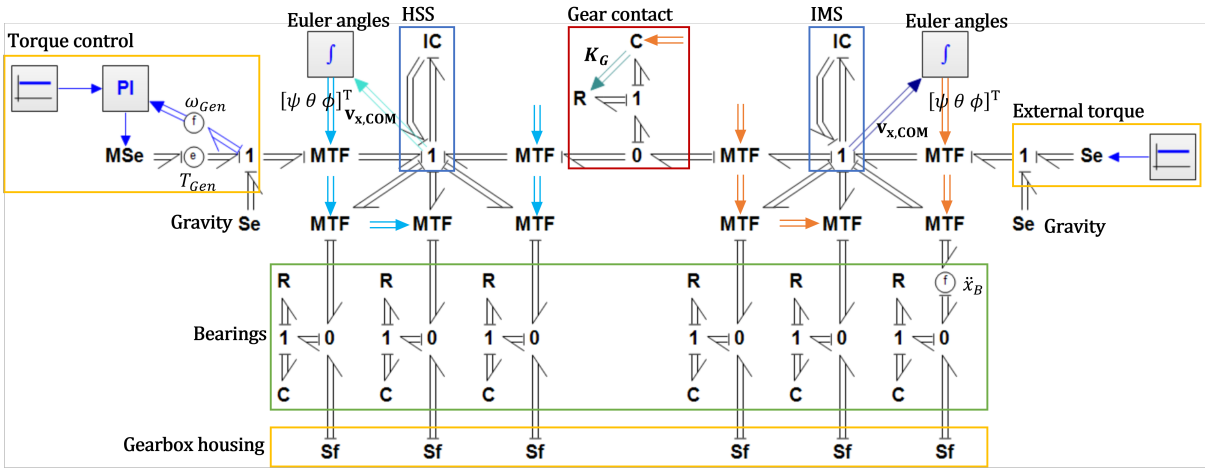

Figure 3. Bond graph structure of high-speed gear stage model

connections to the static gearbox housing. Gear wheel and pinion are rigidly connected to their respective shafts (0 DOF). The elasticity of gear bodies and teeth is lumped into a spring-damper element with time-variant mesh stiffness connecting pinion and gear wheel. External loads T_{in} are applied on the IMS, while a PI-controller sets the desired speed of the HSS with the counter-acting generator torque T_{Gen}.
The key difference between BG and reference model lies in the gear contact formulation, which in SIMPACK is realized with the built-in force subroutine 225. The subroutine incorporates an algorithm to find the 3D contact points and respective surface normal vectors of gear tooth pairings. The contact forces are then determined as a function of relative contact displacement. Hence, the SIMPACK subroutine is able to capture non-linear effects of backlash, micro geometry (profile modifications) and misalignment of shaft axes. Contact stiffness is load-dependent and accounts for gear wheel body deformation stiffnesses, tooth bending and shear stiffnesses, and Hertzian contact stiffness using the 'Weber/ Banaschek' approach. In comparison, the BG model employs a simplified contact formulation, which assumes ideal, kinematic meshing, as presented in Sec. 2.3.4.

2.3. Bond graph model

In the following sections the BG model of a wind turbine high-speed gear stage is presented consisting of submodels of the shafts (Sec. 2.3.2), bearings (Sec. 2.3.3) and helical gear contact (Sec. 2.3.4). The underlying model equations of each submodel given and the graphical representation as BG structure is shown in Fig. 3.

2.3.1. Coordinate systems and transformations The BG model relies on different coordinate systems in the body fixed and inertial frame. The formulation of shaft inertia is most convenient with body-fixed velocities $\mathbf{v_x} \in \mathbb{R}^{6\times1}$ comprising of lateral and angular velocities (Eq. 1), while the boundary conditions align with the inertial frame

$$\mathbf{v_x} = [\mathbf{v_1}, \mathbf{v_2}]^T = [v_x, v_y, v_z, \omega_x, \omega_y, \omega_z]^T. \tag{1}$$

Transformation from body-fixed $\mathbf{v_x}$ to inertial velocities $\mathbf{v_X}$ is realized by three consecutive rotations around the Euler angles ψ (yaw), θ (pitch), ϕ (roll) [15]

$$\mathbf{v_X} = \mathbf{m}_{\psi\theta\phi} \cdot \mathbf{v_x}, \quad \mathbf{m}_{\psi\theta\phi} = \begin{bmatrix} \mathbf{R}_\psi\mathbf{R}_\theta\mathbf{R}_\phi & \mathbf{0} \\ \mathbf{0} & \mathbf{R}_\psi\mathbf{R}_\theta\mathbf{R}_{\phi.} \end{bmatrix}, \tag{2}$$

Table 1. Geometric parameters.

Variable	Symbol	Unit	Value	
			IMS	HSS
Mass	m	[kg]	5059.26	350.89
Moments of inertia	$J_{xx}/J_{yy}/J_{zz}$	[kg · m^2]	994.1 / 723.7 / 723.7	4.6 / 11.1 / 11.1
Number of teeth	z	[-]	95	24
Normal modul	m_n	[mm]	14	
Axis distance	a	[mm]	861	
Gear tooth width	b	[mm]	360	
Operating pitch radius	r_w	[mm]	687.4	173.6
Base radius	r_b	[mm]	633.4	160.0
Tip radius	r_a	[mm]	697.7	190.3
Pressure angle	α	[deg]	20	
Helix angle	β	[deg]	10	
Operating pressure angle	α_w	[deg]	22.86	
Transversal operating pressure angle	α_{wt}	[deg]	22.54	
Number of gear tooth slices	N	[-]	11	
Gear contact stiffness	k_G	[N/m]	$4.69 \cdot 10^8$	
Slope of gear contact stiffness function	$\partial K/\partial \phi^i$	[N/m/deg]	116	
Gear damping to stiffness ratio	ξ	[s]	10^{-3}	

with the individual rotational matrices

$$\mathbf{R}_\psi = \begin{bmatrix} \cos\psi & -\sin\psi & 0 \\ \sin\psi & \cos\psi & 0 \\ 0 & 0 & 1 \end{bmatrix}, \quad \mathbf{R}_\theta = \begin{bmatrix} \cos\theta & 0 & \sin\theta \\ 0 & 1 & 0 \\ -\sin\theta & 0 & \cos\theta \end{bmatrix}, \quad \mathbf{R}_\phi = \begin{bmatrix} 1 & 0 & 0 \\ 0 & \cos\phi & -\sin\phi \\ 0 & \sin\phi & \cos\phi \end{bmatrix}. \tag{3}$$

The time-variant Euler angles are found by integration of body-fixed angular velocities

$$\begin{aligned} \dot{\theta} &= \cos(\phi)\omega_y - \sin(\phi)\omega_z, \\ \dot{\psi} &= \frac{\sin(\phi)}{\cos(\theta)}\omega_y + \frac{\cos(\phi)}{\cos(\theta)}\omega_z, \\ \dot{\phi} &= \omega_x + \sin(\phi)\tan(\theta)\omega_y + \cos(\phi)\tan(\theta)\omega_z \end{aligned} \tag{4}$$

In addition to rotational Euler transformations, lateral transformations are necessary, for instance to relate velocities at bearings with center of mass velocities. The lateral change of coordinate systems from a point A to B is expressed as

$$\mathbf{v_B} = \mathbf{m_{A\to B}} \cdot \mathbf{v_A}, \quad \mathbf{m_{A\to B}} = \begin{bmatrix} \mathbf{I} & -[\delta_{\mathbf{A}\to\mathbf{B}}]_\times \\ \mathbf{0} & \mathbf{I} \end{bmatrix}. \tag{5}$$

The notation $[\cdot]_\times$ is used for compact matrix representation of the cross product between two vectors ($[\mathbf{a}]_\times \mathbf{b} = \mathbf{a} \times \mathbf{b}$). The rotational and lateral transformation matrices $\mathbf{m}_{\psi\theta\phi}$, $\mathbf{m_{A\to B}}$ are orthogonal and thus power-conserving, which are represented in bond graph terminology by transformer elements (TF). In the case of Euler transformation, the transformation matrix is time-variant and a function of the continuously changing Euler angles. Hence, a modulated transformer element (MTF) is used here (Fig 3).

Table 2. Bearing parameters.

Variable	Symbol	Unit	Value					
			IMS-A	IMS-B	IMS-C	HSS-A	HSS-B	HSS-C
Bearing stiffness	K_{xx}	$[\mathrm{N \cdot m^{-1}}]$	0	$7.41 \cdot 10^7$	$7.87 \cdot 10^7$	$1.26 \cdot 10^8$	$6.70 \cdot 10^7$	$7.93 \cdot 10^7$
	K_{yy}	$[\mathrm{N \cdot m^{-1}}]$	$6.12 \cdot 10^7$	$5.17 \cdot 10^8$	$7.37 \cdot 10^8$	$8.21 \cdot 10^8$	$8.09 \cdot 10^8$	$1.04 \cdot 10^9$
	K_{zz}	$[\mathrm{N \cdot m^{-1}}]$	$1.16 \cdot 10^9$	$4.84 \cdot 10^8$	$3.26 \cdot 10^8$	$8.21 \cdot 10^8$	$1.33 \cdot 10^8$	$7.29 \cdot 10^7$
Bearing damping	D_{xx}	$[\mathrm{N \cdot m^{-1} \cdot s}]$	$4.53 \cdot 10^4$					
	D_{yy}	$[\mathrm{N \cdot m^{-1} \cdot s}]$	$4.20 \cdot 10^4$					
	D_{yy}	$[\mathrm{N \cdot m^{-1} \cdot s}]$	$3.06 \cdot 10^4$					
Axial position	x_B	[mm]	-230	230	260	-230	230	260

2.3.2. Shaft model Each gear shaft is considered a rigid body in six DOF. The equations of motion (EOM) governing rigid bodies are derived with the Langrange-Hamiltonian method, which yields second order differential equations for each shaft [15]

$$\mathbf{M}\dot{\mathbf{v}} + \mathbf{C}(\mathbf{v})\mathbf{v} = \tau, \tag{6}$$

where $\mathbf{M} \in \mathbb{R}^{6\times6}$ denotes the mass matrix, $\mathbf{C}(\mathbf{v}) \in \mathbb{R}^{6\times6}$ the coriolis matrix, $\mathbf{v} \in \mathbb{R}^{6\times1}$ the velocity vector and $\tau \in \mathbb{R}^{6\times1}$ the vector of external forces. It is convenient to align the coordinate system with the body-fixed, principal axes at the center of mass ($\mathbf{v} = \mathbf{v_{x,COM}}$) to eliminate off-diagonal elements in the mass matrix, which then becomes

$$\mathbf{M} = \begin{bmatrix} m\mathbf{I} & \mathbf{0} \\ \mathbf{0} & \mathbf{J} \end{bmatrix}, \quad \mathbf{J} = \begin{bmatrix} J_{xx} & 0 & 0 \\ 0 & J_{yy} & 0 \\ 0 & 0 & J_{zz} \end{bmatrix}, \tag{7}$$

where m represents the body mass, $\mathbf{J}$ the moments of inertia and $\mathbf{I} \in \mathbb{R}^{3\times3}$ denotes the identity matrix. The coriolis matrix can then be expressed with Eq. 1 as

$$\mathbf{C} = \begin{bmatrix} \mathbf{0} & -m[\mathbf{v_1}]_\times \\ -m[\mathbf{v_1}]_\times & -[\mathbf{J}\mathbf{v_2}]_\times \end{bmatrix}. \tag{8}$$

The coupled, second order EOM (Eq. 6) can be reformulated as a set of first order differential equations (Lagrange-Hamiltonian form) with the unknowns of generalized displacements $\mathbf{q}$ and momenta $\mathbf{p}$

$$\begin{aligned} \dot{\mathbf{q}} &= \mathbf{M^{-1}}\mathbf{p} \\ \dot{\mathbf{p}} &= -\mathbf{C}(\dot{\mathbf{q}})\dot{\mathbf{q}} + \tau \end{aligned} \tag{9}$$

This relationship is represented with an IC-field in the BG model, highlighted in blue in Fig. 3. Velocities $\dot{\mathbf{q}}$ are determined according to the constitutive laws of a classical I-field (Eq. 9, line 1). Then, gyroscopic forces $\mathbf{e}' = \dot{\mathbf{p}}$ are computed as a function of given velocities in the fashion of a C-field (Eq. 9, line 2) [16].

2.3.3. Bearing model The gear shafts are connected with bearings to the gearbox housing, which is considered static in the inertial frame ($\mathbf{v_0} = \mathbf{0}$). Supporting bearing forces are determined by relative velocities $\Delta\mathbf{v_{X,B}}$ given by local shaft velocities $\mathbf{v_{X,B}}$ at the respective bearing seats

$$\Delta\mathbf{v_{X,B}} = \mathbf{v_{X,B}} - \mathbf{v_0} = \mathbf{v_{X,B}} \tag{10}$$

The local, inertial shaft velocities $\mathbf{v_{X,B}}$ are related to body-fixed velocities $\mathbf{v_{x,COM}}$ at the center of mass through consecutive Euler and lateral transformations

$$\mathbf{v_{X,B}} = \mathbf{m}_{\psi\theta\phi}\mathbf{m_{COM\rightarrow B}} \cdot \mathbf{v_{x,COM}}, \quad \delta_{\mathbf{COM\rightarrow B}} = \begin{bmatrix} x_B \\ 0 \\ 0 \end{bmatrix}. \tag{11}$$

Bearings are considered parallel spring-dampers with diagonal stiffness matrices $\mathbf{K_B}$ and damping matrices $\mathbf{D_B}$. The elastic force component $\mathbf{f_{B,K}}$ is proportional to the relative displacement, which is obtained by integration of relative velocities

$$\mathbf{f_{B,K}} = \mathbf{K_B} \int \Delta\mathbf{v_{X,B}}\ \mathrm{dt}, \quad \mathbf{K_B} = \begin{bmatrix} K_{xx} & 0 & 0 \\ 0 & K_{yy} & 0 \\ 0 & 0 & K_{zz} \end{bmatrix}. \tag{12}$$

The damping force component $\mathbf{f_{B,D}}$ is expressed as follows

$$\mathbf{f_{B,D}} = \mathbf{D_B} \cdot \Delta\mathbf{v_{X,B}}\ , \quad \mathbf{D_B} = \begin{bmatrix} D_{xx} & 0 & 0 \\ 0 & D_{yy} & 0 \\ 0 & 0 & D_{zz} \end{bmatrix}. \tag{13}$$

Bearings are represented with a combination of C- and R-elements for their energy storing (elastic) and the dissipative (damping) capabilities, as shown in green in Fig. 3.

2.3.4. Helical gear contact model The helical gear contact is modelled with a parallel spring-damper connection with a time-variant contact stiffness. The tooth flanks are evenly discretized in N slices with superscript i to account for the uneven load distribution. The contact forces are calculated for each slice separately and are a function of relative, normal velocities $\Delta v^{\mathrm{i}}_{\mathrm{X,CPn}}$ in the teeth contact points CP

$$\Delta v^{\mathrm{i}}_{\mathrm{X,CPn}} = (v^{\mathrm{i}}_{\mathrm{X,CPn}})_{\mathrm{HSS}} - (v^{\mathrm{i}}_{\mathrm{X,CPn}})_{\mathrm{IMS}}. \tag{14}$$

To obtain the velocity component normal to the tooth's surface, the assumption of ideal, kinematic meshing is taken. Under kinematic meshing the normal surface vector and thus the contact force vector is aligned with the line of action at all times. The line of action connects the base circles of gear and pinion and can be expressed in terms of the operating pressure angle α_w and the helix angle β. The normal velocity component $v^{\mathrm{i}}_{\mathrm{X,CPn}}$ is then given by

$$\begin{aligned} v^{\mathrm{i}}_{\mathrm{X,CPn}} &= \mathbf{m_{CPn}}\ \mathbf{v^i_{X,CP}}, \\ \mathbf{m_{CPn}} &= \begin{bmatrix} -\sin(\beta) & \sin(\alpha_w)\cos(\beta) & \cos(\alpha_w)\cos(\beta) & 0 & 0 & 0 \end{bmatrix}. \end{aligned} \tag{15}$$

The inertial velocities in the contact points $\mathbf{v^i_{X,CP}}$ are related to body-fixed, COM velocities $\mathbf{v_{x,COM}}$ through lateral and Euler transformations

$$\mathbf{v^i_{X,CP}} = \mathbf{m}_{\psi\theta\phi}\mathbf{m^i_{COM\rightarrow CP}} \cdot \mathbf{v_{x,COM}}. \tag{16}$$

The contact points are defined in the center of each tooth slice with radial distance of r_w (operating pitch radius) to the COM. The relative distance $\delta^{\mathbf{i}}_{\mathbf{COM\rightarrow CP}}$ for the lateral transformation can be expressed as follows

$$\delta^{\mathbf{i}}_{\mathbf{COM\rightarrow CP}} = \begin{bmatrix} x^i_{CP} \\ y_{CP} \\ z_{CP} \end{bmatrix} = \begin{bmatrix} (i - \frac{N+1}{2})\frac{b}{N} \\ -\cos(\phi) r_w \\ \sin(\phi) r_w \end{bmatrix}. \tag{17}$$

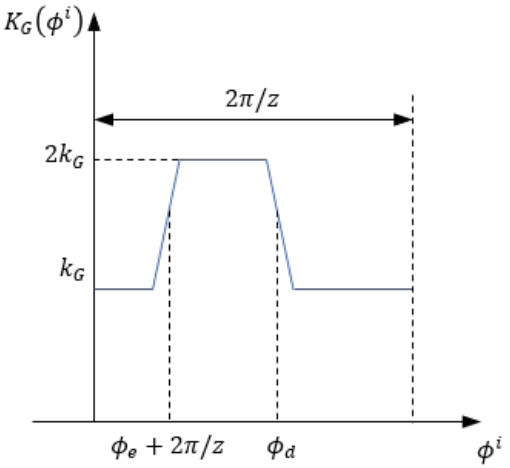

Figure 4. Gear contact stiffness as a function of gear slice angular position ϕ^i and periodical for each meshing period $2\pi/z_1$.

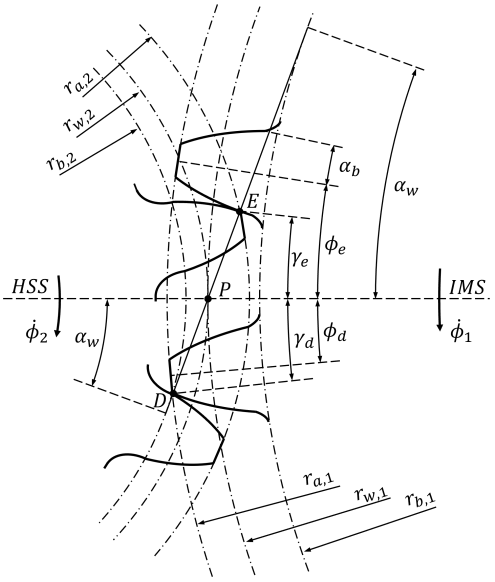

Figure 5. Geometric relations defining the angular position ϕ_e, ϕ_d of the IMS when tooth pairings engage and disengage.

The elastic gear contact forces $f^{\mathrm{i}}_{\mathrm{G,K}}$ are a function of the relative contact displacements obtained by integration and time-variant contact stiffness

$$f^{\mathrm{i}}_{\mathrm{G,K}} = K^i_G(\phi^i) \int \Delta v^{\mathrm{i}}_{\mathrm{X,CPn}} \, \mathrm{dt}. \tag{18}$$

Additionally, stiffness proportional damping is considered in the gear contacts. The damping forces $f^{\mathrm{i}}_{\mathrm{G,D}}$ are a function of relative contact velocities, where the damping coefficient is $D^i_G(\phi^i)$ is assumed proportional to the contact stiffness

$$\begin{aligned} f^{\mathrm{i}}_{\mathrm{G,D}} &= D^i_G(\phi^i) \Delta v^{\mathrm{i}}_{\mathrm{X,CPn}} \\ D^i_G(\phi^i) &= \xi K^i_G(\phi^i). \end{aligned} \tag{19}$$

The formulation of the contact stiffness takes the periodical change in the number of actively engaging teeth into account. For this model with a transverse contact ratio of 1.48 either one or two teeth are in contact simultaneously. As depicted in Fig. 4 the contact stiffness is formulated as a piece-wise linear function of the gear angle ϕ^i switching from a value of k_G, when one tooth is in contact, to $2k_G$, when two teeth are in contact. For improved numerical properties the discrete step in contact stiffness is smoothed with a linear function. The gear angles ϕ^i of each slice are shifted relative to the shaft Euler angle ϕ_1 due to the helical shaping of gear teeth

$$\phi^i = \left(\phi_1 - \frac{x^i_{CP}}{r_w} \tan(\beta) \right) \bmod \frac{2\pi}{z_1}. \tag{20}$$

The gear angles ϕ_e, ϕ_d, at which the contact stiffness function changes values are defined by the engaging and disengaging contact points E and P, as shown in Fig. 5. Under the assumption of ideal, kinematic meshing, E and P are positioned in the intersections of tip radii and the line of action. Using geometric relations, ϕ_e, ϕ_d can be derived as a function of only time-invariant,

geometric parameters

$$\begin{aligned}\phi_{e,d} &= \tan(\gamma_{e,d} + \alpha_w) - \alpha_w - \alpha_b,\\ \alpha_b &= \frac{\pi}{2z_1} + \tan(\alpha_w) - \alpha_w,\\ \sin(\gamma_e) &= -\frac{\cos(\alpha_w)\sqrt{r_{a,1}^2 - r_{b,1}^2} - \sin(\alpha_w) r_{w,1}}{r_{a,1}},\\ \sin(\gamma_d) &= \frac{\cos(\alpha_w)\sqrt{r_{a,2}^2 - r_{b,2}^2} - \sin(\alpha_w) r_{w,2}}{r_{a,1}}.\end{aligned} \tag{21}$$

where $\gamma_{e,d}$ are auxiliary parameters, α_w denotes the operating pressure angle, α_b the half angle of tooth thickness on the base circle, z_1 the tooth number and r_a, r_b, r_w the tip, base and pitch radii respectively.
Analogously to the bearing model, the gear contact model comprises of an energy storing C-element and dissipative R-element representing stiffness and damping forces, as indicated in red in Fig. 3.

2.3.5. Boundary conditions The gear stage is under load from external sources such as aerodynamic excitations. In this model all external loads are applied at the IMS's center of mass, while a PI-controller provides the counter-acting generator torque to reach the desired HSS speed. External loads and generator torque constitute force boundary condition and are represented by effort source elements (Se) in the bond graph structure (Fig. 3, yellow). Furthermore, the model assumption of a static gearbox housing sets a zero velocity boundary condition, which is represented with flow source elements (Sf).

2.4. Model Integration in Digital Twin Framework
This section provides an outlook on the integration of the presented BG model in the envisioned DT framework, shown in Fig. 1. State estimation methods such as the Extended Kalman Filter (EKF) are employed to synchronize the virtual model with the physical turbine on the basis of physical sensor measurements. These require a mathematical description of the virtual model in the form of state-transition function $\mathbf{f}(\mathbf{x}, \mathbf{u})$, and measurement function $\mathbf{g}(\mathbf{x}, \mathbf{u})$

$$\begin{aligned}\dot{\mathbf{x}} &= \mathbf{f}(\mathbf{x}, \mathbf{u}),\\ \mathbf{y} &= \mathbf{g}(\mathbf{x}, \mathbf{u}).\end{aligned} \tag{22}$$

The independent state variables $\mathbf{x}$ can be identified from the BG structure (Fig. 1) as the momenta $\mathbf{p_1}, \mathbf{p_2}$ of each shaft, displacements of bearings $\mathbf{q_B}$ and gear slices $\mathbf{q_G}$ and euler angles $[\psi, \theta, \phi]_{1,2}^T$

$$\mathbf{x} = [\mathbf{p_1}, \mathbf{p_2}, \mathbf{q_B}, \mathbf{q_G}, \psi_1, \theta_1, \phi_1, \psi_2, \theta_2, \phi_2,]^T. \tag{23}$$

The measurement variables $\mathbf{y}$ include the HSS rotational speed ω_{gen} and the generator torque T_{gen} from SCADA data, as well as bearing accelerations $\ddot{x}_B$ from CMS vibration data. In the virtual model the interface to these physical measurements is represented with effort (e) and flow (f) sensors (Fig. 1)

$$\mathbf{y} = [\omega_{gen}, T_{gen}, \ddot{x}_B]^T. \tag{24}$$

The state equations (Eq. 22) can be derived analytically using the systematic procedure of the BG method or automatically generated with the BG software 20sim [17]. 20sim supports the export as executable MATLAB functions, which can be referenced by an EKF implemented in

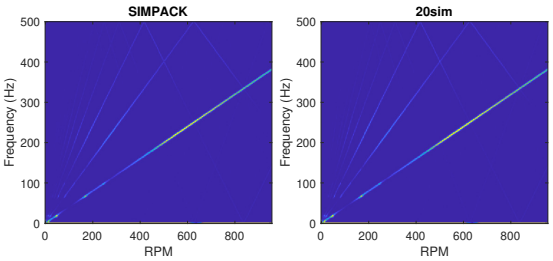

Figure 6. Run-up spectrogram of angular velocity ω_X of IMS. l.: reference model (SIMPACK), r.: bond graph model (20sim)

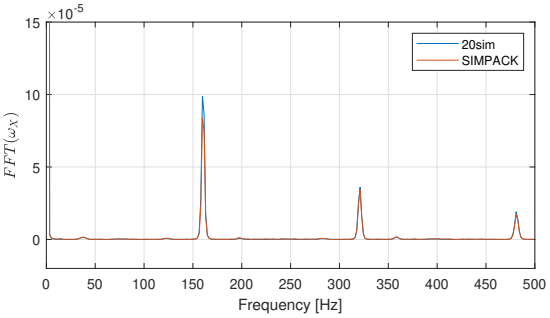

Figure 7. Slice of run-up spectrogram (Fig. 6) at 400 rpm.

MATLAB. The EKF is extended to incorporate virtual sensors for estimation of gear and bearing loads by augmenting the state vector similar to the approach of Branlard et al. [18]. Preliminary studies show compatibility of the BG model with the proposed virtual sensing method, however analysis and verification is part of future work.

3. Results and Discussion

3.1. Model validation

Validation of the BG model is conducted with the reference model implemented in SIMPACK (Sec. 2.2) under two basic load cases: run-up from standstill to rated speed $n_{gen} = 1165.94$ rpm and a stationary load case at rated speed. Under each load case the gear stage is loaded with rated torque of $T_{in} = 162.1$ kNm at the IMS.

The torsional system dynamics are evaluated in the run-up load case using the angular velocity ω_X of the IMS. As evident from the spectogram depicted in Fig. 6, the bond graph model displays dynamic behaviour similar to the reference model. The bright line indicates excitation from gear meshing at the mesh frequency $f_{mesh} = n_{gen}/60 \cdot z_{HSS}$, while the darker lines show higher harmonics ($2\times f_{mesh}, 3\times f_{mesh}$). The decreasing line segments can be attributed to aliasing effects, since the higher harmonics exceed the Nyquist frequency of 500 Hz here. Resonance can be observed at particular shaft speeds where the gear meshing frequency coincides with the system's natural frequencies. As shown in Tab. 3 the natural frequencies of both models match with a relative error of less than 2%. A slice through the spectrogram at a shaft speed of 400 rpm also shows a good agreement in the amplitudes of ω_X.

The stationary load case allows a closer look at time series of gear contact forces and bearing forces. Shown in Fig. 8 are gear contact forces at the left edge slice 1, center slice 6 and right edge slice 11. The bond graph model is able to accurately reproduce the inhomogeneous load distribution over the tooth flank, as well as the cyclic compression and decompression for each meshing period. The mean values of gear forces agree well across all slices with a maximum error of 5.6%, while the amplitudes appear to be overestimated by up to 22.0% at the left edge slice.

Axial and radial forces of bearing HSS-A are selected as representatives for bearing behaviour (Fig. 9). Bearing forces have a large stationary component due to supporting a stationary gear stage torque and an oscillatory component induced by gear meshing. The error in mean value of forces is below 2.0% for all gear stage bearings, however force amplitudes differ by up to 37.1%.

Table 3. First five non-trivial eigen frequency pairs of bond graph model (20sim) and reference model (SIMPACK).

f_i [Hz]	$f_{4/5}$	$f_{6/7}$	$f_{8/9}$	$f_{10/11}$	$f_{12/13}$	$f_{14/15}$
SIMPACK	5.98	19.14	27.56	67.05	98.93	105.5
20sim	6.06	19.13	27.66	67.16	98.74	106.5

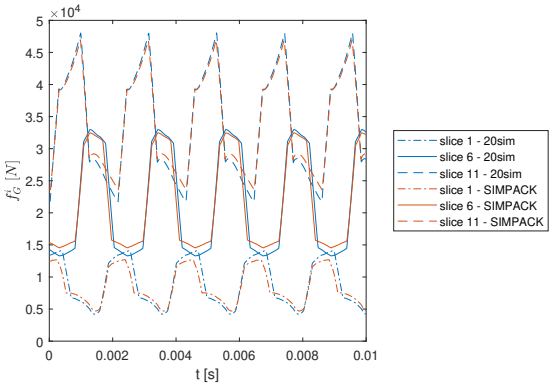

Figure 8. Gear contact forces at rated speed and torque for bond graph model (20sim) and reference model (SIMPACK).

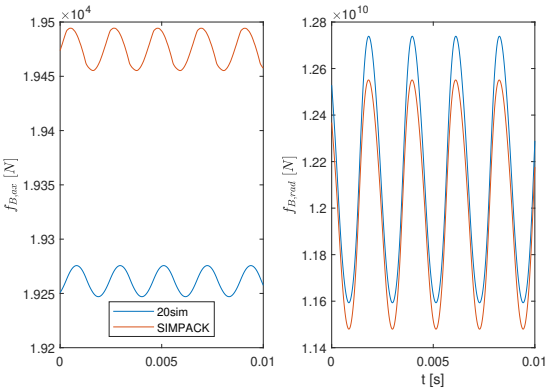

Figure 9. Axial and radial bearing forces at HSS-A at rated speed and torque for bond graph model (20sim) and reference model (SIMPACK).

3.2. Computational speed

Since the BG model is intended for real-time simulation in DT, it is important to consider the computational efficiency. A real-time factor of $t_{CPU}/t_{real} = 3.0$ is measured with the BG model and $t_{CPU}/t_{real} = 4.1$ with the reference model in SIMPACK, when simulating the stationary load case on a desktop computer. The explicit solver Runge-Kutta 4 is used for simulation of the BG model, while for the reference model the default SIMPACK solver SODASRT2, an implicit backward differential solver is used. Admittedly, real-time capability is not reached with the BG model, however an improvement in computational speed can be observed. Further investigations on optimizing the computational performance are planned. One numerically advantageous property of the BG model is the absence of any algebraic loops. Algebraic loops are circular dependencies of state variables and result in constraint equations of the form $\mathbf{0} = \mathbf{h}(\mathbf{x}, \mathbf{u})$, which have to be solved iteratively for each time step adding to the computational cost. In the BG model algebraic loops are avoided by modelling gear contact forces explicitly as a function of body velocities (Eq. 18). The gear contact model in SIMPACK on the other hand is formulated implicitly, as the position of tooth contacts and the resultant force vector orientation are calculated iteratively

4. Conclusion

In this paper a wind turbine high-speed gear stage model for the purpose of for real-time virtual sensing of gear and bearing loads in a DT framework was presented. The model was developed with the energy-based BG method and implemented in the software 20sim for numerical integration. The BG method provides a systematic approach to derive state equations, which are required for the state estimating methods employed in virtual sensors. The model fidelity is close to state-of-the-art MBS models considering 6 DOF rigid body motion,

however a simplified gear contact formulation with the assumption of ideal, kinematic meshing is used. Nonetheless, comparative simulations with a with a reference model implemented in MBS software SIMPACK show good agreement in gear contact and bearing loads in a stationary and a run-up load case. Errors in mean value are below 5.6% and 2.0% for gear and bearing forces respectively. Force amplitudes are overestimated by the BG model with maximum errors of 22.0% and 37.1%. The BG model shows favourable computational performance with a real-time factor of 3.0 as opposed to 4.1. This is likely a result of the explicit gear contact formulation, which avoids computationally expensive iterations to find contact displacements. The results suggest that the developed model is capable and suitable for the proposed virtual load sensing approach. Further investigations are planned on the analysis and verification of this approach.

Acknowledgments

The authors wish to acknowledge financial support from the Research Council of Norway through InteDiag-WTCP project (Project number 309205).

References

[1] Stehly T and Beiter P 2020 2018 cost of wind energy review Report National Renewable Energy Laboratory
[2] Rasheed A, San O and Kvamsdal T 2020 *IEEE Access* **8** 21980–22012 ISSN 2169-3536
[3] Tao F, Zhang M, Liu Y and Nee A Y C 2018 *CIRP Annals* **67** 169–172 ISSN 00078506
[4] Moghadam F K and Nejad A R 2020 *Journal of Physics: Conference Series* **1618**
[5] Mehlan F C, Nejad A R and Gao Z *International Conference on Ocean, Offshore and Arctic Engineering* **9**
[6] Moyne J, Qamsane Y, Balta E C, Kovalenko I, Faris J, Barton K and Tilbury D M 2020 *IEEE Access* **8** 107781–107801 ISSN 2169-3536
[7] Guo Y, Keller J, Cava W L, Austin J, Nejad A R, Halse C, Bastard L and Helsen J 2015 *Conference for Wind Power Drives (CWD)*
[8] Matzke Dand Schelenz R, Reisch S, Roscher B, Jacobs G; Theling J, Schroers M, Loepenhaus C and Brecher C 2018 *Journal of Physics: Conference Series* **1037**
[9] Nejad A R, Guo Y, Gao Z and Moan T 2016 *Wind Energy* **19** 1089–1106 ISSN 10954244
[10] Wang S, Nejad A R and Moan T 2020 *Wind Energy* **23** 1099–1117 ISSN 1095-4244 1099-1824
[11] Nejad A R, Keller J, Guo Y, Sheng S, Polinder H, Watson S, Dong J, Qin Z, Ebrahimi A, Schelenz R, Guzmán F G, Cornel D, Golafshan R, Jacobs G, Blockmans B, Bosmans J, Pluymers B, Carroll J, Koukoura S, Hart E, McDonald A, Natarajan A, Torsvik J, Moghadam F K, Daems P J, Verstraeten T, Peeters C, and Helsen J 2022 *Wind Energ. Sci.* **7**(1)
[12] Li X and Zhang W 2022 *Renewable Energy* **185** 932–944 ISSN 09601481
[13] URL `https://www.3ds.com/products-services/simulia/products/multibody-system-simulation/`
[14] Karnopp D C, Margolis D L and Rosenberg R C 1990 *Modeling, Simulation, and Control of Mechatronic Systems* System dynamics (John Wiley Sons, Inc)
[15] Pedersen E 2009 *Mathematical and Computer Modelling of Dynamical Systems* **15** 337–352 ISSN 1387-3954 1744-5051
[16] Karnopp D 1992 *Journal of the Franklin Institute* **329** 65–75 ISSN 0016-0032
[17] URL `https://www.20sim.com/`
[18] Branlard E, Giardina D and Brown C S D 2020 *Wind Energy Science* **5** 1155–1167 ISSN 2366-7451